ORIGINAL RESEARCH

eurasia

Alkali (Na/K) Doped Cobalt Ferrite Nanoparticles: Photocatalytic and Antioxidant Activities

Article History
Received: 21-Mar-2025
Revised: 30-May-2025
Accepted: 3-Jun-2025
Published: 15-Jul-2025

Shaweta Chandel[a,c], Shweta. Kaushal[a,c], Naveen Thakur[b,c], Sandeep Kumar[d], Kuldeep Kumar[*a,c]

Abstract: Nanotechnology has been a constant subject of innovation in the past two decades. Novel innovations have been carried out to enhance the properties of nanoparticles, especially by doping. It is one of the main ways to augment the properties of a semiconductor. In the present paper, alkali (Na/K) doped cobalt ferrite nanoparticles (NPs) were successfully synthesized and investigated for their effectiveness for photocatalytic degradation of Methylene Blue (MB) and Methyl Orange (MO), as well as antioxidant properties. So obtained Na/K doped $CoFe_2O_4$ were characterised for the evaluation of their structural, elemental, morphological, and optical criteria via using standard characterisation methods like XRD, SEM, EDX, TEM, and UV-Visible spectroscopy. The XRD results showed the crystallite size of Na-doped $CoFe_2O_4$ to be between 25 to 26 nm, while that for K-doped it was between 15 to 16 nm. The smaller crystallite size of K-doped particles can be attributed to the fact that K has a larger ionic radius than Na and causes more lattice strain, disrupting the lattice growth. The morphological variations with the dopants and elemental composition have been confirmed by using SEM-EDS and TEM results. The UV-Visible results implied the absorption regions for Na/$CoFe_2O_4$ with band gap energy between 1.65 to 1.5 eV, while for K/$CoFe_2O_4$ it is between 1 to 1.41 eV. Based on the results, it was established that K/$CoFe_2O_4$ exhibited greater photocatalytic and antioxidant properties.

Keywords: Alkali metal, Antioxidant activity; Doped ferrites; Photocatalytic activity

a Department of Chemistry, Career Point University, Hamirpur, Himachal Pradesh, 176041, India

b Department of Physics, Career Point University, Hamirpur, Himachal Pradesh, 176041, India

c Center for Nano-Science and Technology, Career Point University, Hamirpur, Himachal Pradesh, 176041, India

d ICAR-Indian Agricultural Research Institute, Regional Station, Katrain, Himachal Pradesh, 175129, India.

ORCID: Kuldeep Kumar: 0000-0003-4055-5011

* **Corresponding author:** Email: kuldeep.sharma.753@gmail.com

1. INTRODUCTION

In the past two decades, there has been immense research in nanotechnology. A lot of work has been reported around nanotechnology applications. In today's research, the focus is on enhancing the physical and chemical properties of nanoparticles (NPs) to increase their overall applications. Ferrite NPs have been known to have a lot of applications, especially in the biomedical field and photocatalysis (Velayutham et al., 2022). In developing countries, access to clean drinking water is still an issue. With the advent of industrialization, the problem of water pollution has increased manifold, especially regarding the disposal of wastewater. The use of nanotechnology in water cleaning is very effective. By water remediation, we can minimize or remove water contaminants that are detrimental to our ecosystem as well as to human health (Elansary et al., 2024). In the current times, due to immense advancements in nanotechnology, water remediation techniques include nanofiltration methods, nano-adsorbents, the use of nano zero-valent iron, nano biocides, etc. (Khlyustova et al., 2020). Water pollution, especially due to the discharge of organic pollutants like dyes, has been of great concern,

carrying out the process of dye degradation by photocatalysis using metal NPs. Several modifications have been made, and one of them is by doping.

Doping is a physical change and includes the deliberate insertion of one element into the crystal lattice of another element. It is the most compatible method to enhance the characteristics of NPs (Shenoy et al., 2022) and a convenient way of calibration to enhance the properties of NPs with the retention of their high surface areas (M. Matar et al., 2025). As has been reported in the case of TiO_2 NPs, doping with metals leads to shortening of the band gap, which enhances their photocatalytic activity. The improvement in the photonic activity of TiO_2 was observed with the incorporation of dopants, and photocatalytic activity was increased considerably (Girija et al., 2022). Further, it enhances the physical characteristics of NPs, as several NPs require fine-tuning to achieve targeted functions (Albalah et al., 2020). Through a literature survey, it has been reported that the incorporation of Neodymium in CeO_2 (Ceballos-Sanchez et al., 2024), Zirconium in CeO_2 (Rai & Kanagaraj, 2022) increases antioxidant properties. Even modification of NPs with essential oils has been reported to increase their antioxidant properties (López-Cano et al., 2023). After going through all the literature survey it is concluded that doping is a good way to increase antioxidant and photocatalytic activities of NPs and alkali metals act as good dopants as they have low ionisation energies and therefore their valence electrons can be easily introduced to generate an electron excess system (Hameed et al., 2023). Doping with alkali metals has been reported to increase the stability of nanocages in Bi-alkali metal doping, reduce energy gap between HOMO and LUMO (Sohail et al., 2021), improve thermal and moisture stability of NPs (Manjunatha et al., 2024) and can further accelerate light absorption, improve sensing ability of metal sensors (Kausar et al., 2021).

As is well known, antioxidants in general have great significance in various fields. In the human body, they help to reverse the damage caused to cells by oxidation and help in reducing the probability of certain diseases related to the heart, cancer, inflammation of joints, vision loss, Parkinson's, and Alzheimer's disease (Shah et al., 2023). In addition to this, they are used in pharmacology, packaging technology, the food industry, cosmetics, etc., as they help to increase the shelf life of food, prevent discoloration, and increase oxidation stability (Mozafari & Barbati, 2024; Tahir et al., 2015). NPs help antioxidants reach their targets through encapsulation (Khalil et al., 2019), passive and active targeting (Amani et al., 2017; Peng et al., 2025), etc. Antioxidant activity of NPs includes several methods and mechanisms, like scavenging of nitrogen and oxygen species, quenching various free radicals (Samrot & Noel Richard Prakash, 2023), radical trapping (Valgimigli & Pratt, 2015), etc. One of the most significant contributions of NPs is that they can be used to convey antioxidants in a more effective, stable, and targeted manner than natural and feigned antioxidants.

Cobalt Ferrite NPs are of great importance to researchers due to their numerous applications, viz., high coercivity, chemical stability, morphology, crystalline anisotropy, and so on (Tahir et al., 2023). Among various methods used to synthesize NPs, the co-precipitation method leads to good control over particle size and uniformity, thus enhancing their properties (Kanagesan et al., 2016; Zhao et al., 2024). In the present work, we are studying the photocatalytic and antioxidant activity of Na and K-doped Cobalt ferrite NPs. A total of six samples, viz. $Na_{(0.001)}Co_{(0.001)}Fe_2O_{4(0.098)}$, $Na_{(0.001)}Co_{(0.003)}Fe_2O_{4(0.096)}$, $Na_{(0.001)}Co_{(0.005)}Fe_2O_{4(0.094)}$, $K_{(0.001)}Co_{(0.001)}Fe_2O_{4(0.098)}$, $K_{(0.001)}Co_{(0.003)}Fe_2O_{4(0.096)}$, and $K_{(0.001)}Co_{(0.005)}Fe_2O_{4(0.094)}$ have been prepared by keeping the concentration of dopant same in all the samples. The objective of this work is to study and compare the effect of these two alkali metals as dopants. K^+ and Na^+ ions are monovalent and are larger as compared to Co^{2+} and Fe^{3+}, so there is substitutional doping primarily (Jhala et al., 2024) affecting interstitial sites, which leads to significant lattice distortion.

Further, as Cobalt ferrite has an inverse spinel structure, which enhances its a hard ferrite material having moderate magnetizing properties so the introduction of Sodium and Potassium as dopants can lead to modification in its physical and chemical assets by redistributing Co^{2+} and Fe^{3+} ions between tetrahedral (A) and Octahedral sites (B), creation of Oxygen vacancies which increase surface reactivity beneficial for catalysis, and also it enhances biocompatibility which facilitates its biomedical use (Bhardwaj et al., 2024). These potential characteristics make Na and K promising dopants for research, especially for photocatalytic and antioxidant applications. Generally, it has been observed that many transition metals, such as Zn, Mn, Ni, Co, Cu, etc., are common dopants and much work has been reported on them, especially their applicability in altering magnetic properties, electrical conductivity. Amongst alkaline and alkali metal dopants, Mg, Ca, Ba, Sr, and Li are relatively common; most reported applicability is regarding

improving and altering material properties for enhancing resistivity, electrical conductivity, etc. Na and K have been taken as dopants here as they are relatively uncommon, contributing to the novelty of the work, although they are available in abundance, economical, and have low toxicity, which makes them environmentally friendly and a good choice as potential dopants. It is interesting to study how they act as dopants in Cobalt Ferrites. Cobalt Ferrites have photocatalytic and antioxidant properties, and it is relatively novel to compare the effect of doping by Na and K on these properties.

Most of the reported data is based on doping of transition and rare earth metals, and there is a dearth of systematic and comprehensive studies based on doping of Na and K. This study aims to fill these research gaps. Largely, transition metal and rare earth ions have been used as dopants due to their charge balancing, magnetic properties (Kalia & Prasad, 2023) but here, monovalent and non-magnetic ions are being used in a magnetic spinel system, so it will be interesting to investigate their effects and might lead to new insights in the future.

2. MATERIALS AND METHODS

2.1. Materials

All the chemicals like Fe $(NO_3)_3$. $9H_2O$, $Co(NO_3)_2 \cdot 6H_2O$, polyethylene glycol (PEG), $NaNO_3$, KNO_3, KOH, methyl orange (MO), methylene blue (MB), DPPH, and ascorbic acid have been purchased from Merck, India, and no additional purification has been carried out.

2.2. Synthesis of cobalt ferrite NPs

Nanoparticles (NPs) were synthesized using the co-precipitation method, following the procedures described by Houshiar et al. (2014) and Sangsuriyonk et al. (2022), with minor modifications. A total of six samples were prepared with the following compositions: $Na_{(0.001)}Co_{(0.001)}Fe_2O_{4(0.098)}$, $Na_{(0.001)}Co_{(0.003)}Fe_2O_{4(0.096)}$, $Na_{(0.001)}Co_{(0.005)}Fe_2O_{4(0.094)}$, $K_{(0.001)}Co_{(0.001)}Fe_2O_{4(0.098)}$, $K_{(0.001)}Co_{(0.003)}Fe_2O_{4(0.096)}$, and $K_{(0.001)}Co_{(0.005)}Fe_2O_{4(0.094)}$. To prepare $Na_{(0.001)}Co_{(0.001)}Fe_2O_{4(0.098)}$, a 0.098 M solution (3.95871 gm/100 ml) of ferric nitrate nonahydrate $(Fe(NO_3)_3 \cdot 9H_2O)$ was prepared in distilled water. The solution was heated and stirred at 70°C using a magnetic stirrer. Once the temperature stabilized, 100 ml of 0.001 M solution (0.0291 gm/100 ml) of cobalt nitrate hexahydrate $(Co(NO_3)_2 \cdot 6H_2O)$ was added gradually, followed by 100 ml of 0.001 M sodium nitrate ($NaNO_3$) solution (0.008499 gm/100 ml).

For the synthesis of $Na_{(0.001)}Co_{(0.003)}Fe_2O_{4(0.096)}$, the sodium dopant concentration was kept constant at 0.001 M, while the cobalt nitrate concentration was increased to 0.003 M (0.087309 gm/100 ml). Accordingly, the ferric nitrate concentration was adjusted to 0.096 M (3.877 gm in 100 ml) to maintain a total metal ion concentration of 0.1 M. Similarly, $Na_{(0.001)}Co_{(0.005)}Fe_2O_{4(0.094)}$ was prepared using 0.005 M cobalt nitrate (0.1455 gm/100 ml) and 0.094 M ferric nitrate (3.797 gm/100 ml).

The potassium doped cobalt ferrites, $K_{(0.001)}Co_{(0.001)}Fe_2O_{4(0.098)}$, $K_{(0.001)}Co_{(0.003)}Fe_2O_{4(0.096)}$, and $K_{(0.001)}Co_{(0.005)}Fe_2O_{4(0.094)}$ were synthesized using 0.001 M (0.01011 gm/100 ml) potassium salt (KNO_3) as the dopant. The concentrations of cobalt and ferric nitrate used were the same as those in the corresponding sodium doped samples.

It is important to note that in all six samples, the atomic percentage of Na^+ and K^+ is 1%, corresponding to a mole fraction of 0.01. During synthesis, the pH was adjusted to between 11 and 12 using 1 M KOH solution. Approximately 40 ml of base was required to achieve the desired pH. polyethylene glycol (PEG) was used as a surfactant to aid in the uniform dispersion of particles. After pH adjustment, the reaction mixture was stirred continuously for 3 hours. The resulting nanoparticles were washed thoroughly with distilled water and ethanol, then dried in a vacuum oven. Finally, the dried samples were calcined at 800°C for 3 hours.

2.3. Characterization

The formation of the Na/K/$CoFe_2O_4$ samples was tested using spectroscopic techniques. The structural determinations were done by using Powder X-ray diffraction (PXRD). Scanning electron microscope (SEM), Transmission electron microscope (TEM), and energy dispersive X-ray (EDX) were used to determine the morphological attributes and elemental composition. The UV-visible spectrophotometer, ranging from 200–800 nm, was used for checking the absorbance-related properties of the samples.

2.4. Photocatalytic Activity

The photocatalytic activity was tested under irradiation of UV light instead of sunlight, according to

the study by Kumar et al. (2023). A photocatalytic chamber, which consisted of a UV lamp lying 5–7 cm above the reaction mixture. A magnetic stirrer for continuous stirring of the reaction mixture was used to study the photocatalytic activity. This whole apparatus was enclosed inside a dark box so that UV light might not escape the setup. A 100 ml solution of MO and MB was treated with different amounts of (5, 15, and 25 mg) Na/$CoFe_2O_4$ and K/$CoFe_2O_4$ NPs. The reaction was observed over 100 min at an interval of 10 min. It was observed that with the progress of the reaction, there was a decrease in the absorbance of λ_{max} values for MO and MB.

2.5. Antioxidant Activity

The antioxidant properties of NPs are well known. The antioxidant properties of Na/$CoFe_2O_4$ and K/$CoFe_2O_4$ NPs were studied by using the DPPH assay method (Kaushal et al., 2024). DPPH has nitrogen carrying an odd electron, and its stable nature makes it an excellent chemical for studying the radical scavenging activity of antioxidants. The method is based on the spectrophotometric measurement of the change in concentration of DPPH because of its reaction with the antioxidant. A 2 mL methanolic solution was prepared, and DPPH was added at various concentrations (25, 50, 100, 200, 400, 800 µg/ml) through the serial dilution method. After dilution, the samples were kept in the dark for approximately 30 min. The samples were subjected to the UV-visible spectrophotometric technique to chalk out the radical scavenging activity. The wavelength was set at 517 nm. Ascorbic acid was taken as the standard. It is to be noted that the experiment with each of the six samples was repeated three times to have a more concise value of percent scavenging by NPs, and the average values were replicated to have more precision and accuracy.

3. RESULTS AND DISCUSSION

3.1. XRD Results

The XRD analysis confirmed the phase and purity of pure and doped $CoFe_2O_4$ as shown in **Fig. 1**. The diffraction peaks of CoFe2O4 were exhibited at 2θ = 25.4°, 34.19°, 36.86°, 42.21°, 50.65°, 55.37°, 63.59°, and 65.107° which were indexed to the planes 111, 220, 311, 400, 422, 511, 440 and matched well with JCPDS No.- 22-1086 (do Carmo Dias et al., 2024) and the most intense peak was observed at 34.19°. The most intense peak for Na-doped $CoFe_2O_4$ was observed at a little shifted distance, as observed in $Na_{(0.001)}Co_{(0.001)}Fe_2O_{4(0.098)}$, $Na_{(0.001)}Co_{(0.003)}Fe_2O_{4(0.096)}$, and $Na_{(0.001)}Co_{(0.005)}Fe_2O_{4(0.094)}$, where the most intense peak was at 35.35°, 36.52°, and 35.52°, respectively and this is possibly due to the compressional strain that contracts the lattice shifting the peak to a higher angle (Harrington et al., 2021). In the case of K-doped $CoFe_2O_4$ viz $K_{(0.001)}Co_{(0.001)}Fe_2O_{4(0.098)}$, $K_{(0.001)}Co_{(0.003)}Fe_2O_{4(0.096)}$, and $K_{(0.001)}Co_{(0.005)}Fe_2O_{4(0.094)}$ the conspicuous peaks are observed at 33.13, 32.91 and 32.74 degree and which means there is shifting of the peaks to a little lower theta values indicating the expansion to a higher lattice parameter which can be caused by uniform strain (macro strain) throughout the material (Prasetya et al., 2020). Using the Scherer equation (1) and Bragg's relation (2), crystallite size and the interplanar spacing were calculated:

$$D = \frac{K\lambda}{\beta \cos\theta} \quad (1)$$

$$d = \frac{n\lambda}{2\sin\theta} \quad (2)$$

where D is the crystallite size in the direction perpendicular to lattice planes, K is a constant, λ is the x-ray radiation wavelength in Å, θ is the peak angle, β is the FWHM (Full width at half maximum), and d is the interplanar spacing. It was observed from **Table 1** that there has been a decrease in the crystallite size with the incorporation of Na and K as the dopants because larger radius ions replaced smaller radius ions. The decrease in crystallite size upon doping involves various key factors like lattice strain, site occupancy, crystal distortion, inhibition of crystal growth due to the introduction of imperfections and boundaries, and altered surface energy (Barkat et al., 2022; Singha & Singh, 2020). The K-doped $CoFe_2O_4$ has a smaller size, which can be attributed to the fact that the potassium ion has a larger ionic radius than the sodium ion and thus the former creates more lattice strain, which in turn disrupts crystal growth. The K^+ ions cause higher lattice distortion, limiting crystal growth, further in spinel structures K^+ may favour certain sites or interstitial positions that they cannot occupy fully due to size mismatch and this creates structural disorder that hinders regular arrangement and crystal growth (Hossain et al., 2018; Khanna & Verma, 2014). Also, when the concentration of dopant, i.e., Na, remains the same but that of parent constituents increases,

there is an increase in lattice parameter, and the same is the case with K-doped NPs. This can be attributed to the fact that there is reduced atomic packing density as parent molecules occupy lattice sites, increasing lattice, weakened bonding as high parent molecule concentration reduces bond strength, strain relaxation, and electronic structure modification (Nordin et al., 2015; Xiao et al., 2022).

Figure 1. XRD patterns of Na and K-doped cobalt ferrite samples

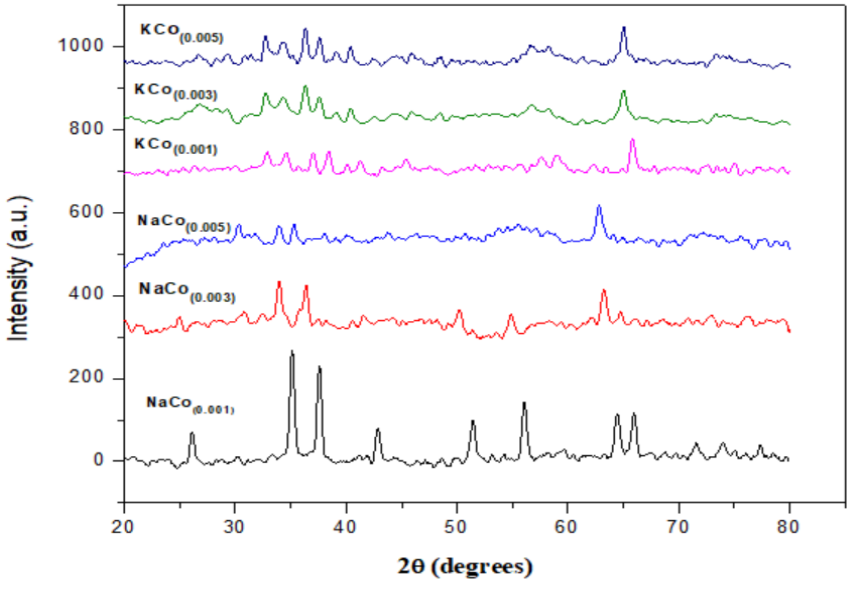

Table 1. Structural parameters for Na and K-doped cobalt ferrite samples

Samples	Crystallite Size (D) (nm)	Interplanar Spacing (d) (nm)	Lattice Parameter
$Na_{(0.001)}Co_{(0.001)}Fe_2O_{4(0.098)}$	25.55	2.085	5.86
$Na_{(0.001)}Co_{(0.003)}Fe_2O_{4(0.096)}$	25.98	2.331	6.00
$Na_{(0.001)}Co_{(0.005)}Fe_2O_{4(0.094)}$	28.63	2.331	7.18
$K_{(0.001)}Co_{(0.001)}Fe_2O_{4(0.098)}$	15.49	2.149	5.80
$K_{(0.001)}Co_{(0.003)}Fe_2O_{4(0.096)}$	15.95	2.178	5.86
$K_{(0.001)}Co_{(0.005)}Fe_2O_{4(0.094)}$	16.18	2.429	5.89

3.2. SEM and EDX Results

SEM-EDX has been carried out to study the morphological and elemental analysis of the samples. The micrographs indicated spherical and irregular morphology of doped NPs (**Fig. 2**). The morphology exhibited by samples doped with Na showed faceted and spherical-like particles (Abd El-Salam et al., 2023). As indicated in **Fig. 2 (d–f)**, the morphology of K-doped cobalt ferrites was irregular with higher surface roughness than Na-doped NPs due to the disruption of uniform crystal growth (Dippong et al., 2023). There is a tendency for agglomeration in K-doped samples of cobalt ferrites due to higher surface energy and strain-induced defects as compared to Na-doped samples, which show less aggregation, leading to better-dispersed particles (López-Ortega et al., 2015). The EDX spectra showed peaks for Na, K, Co, Fe, and O elements in **Fig. 2**. The strong peaks exhibited by elements confirmed the chemical composition of Na and K-doped cobalt ferrites.

Figure 2. SEM-EDX micrographs of Na and K-doped cobalt ferrite (a–f) samples

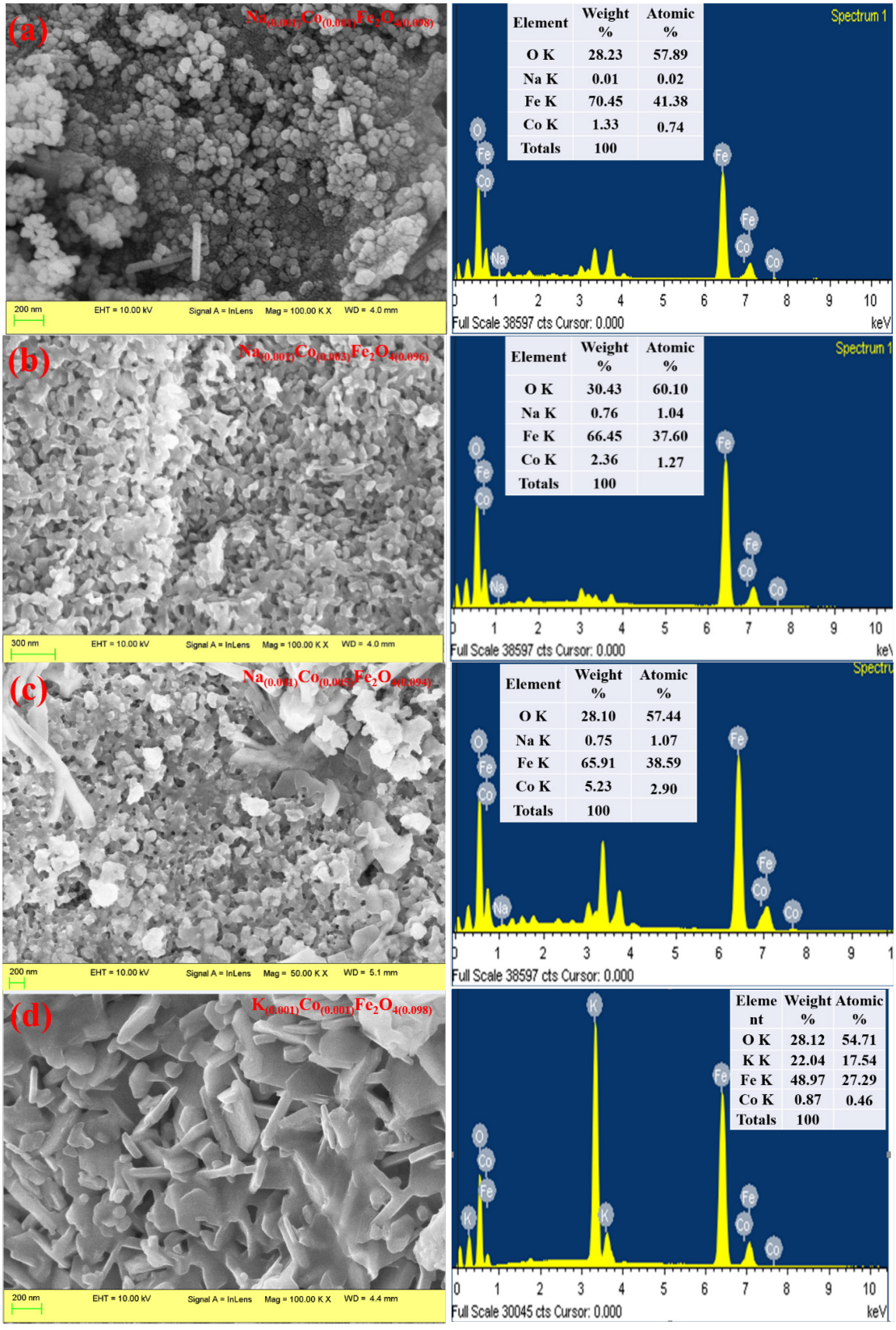

 https://doi.org/10.37819/nanofab.10.2069

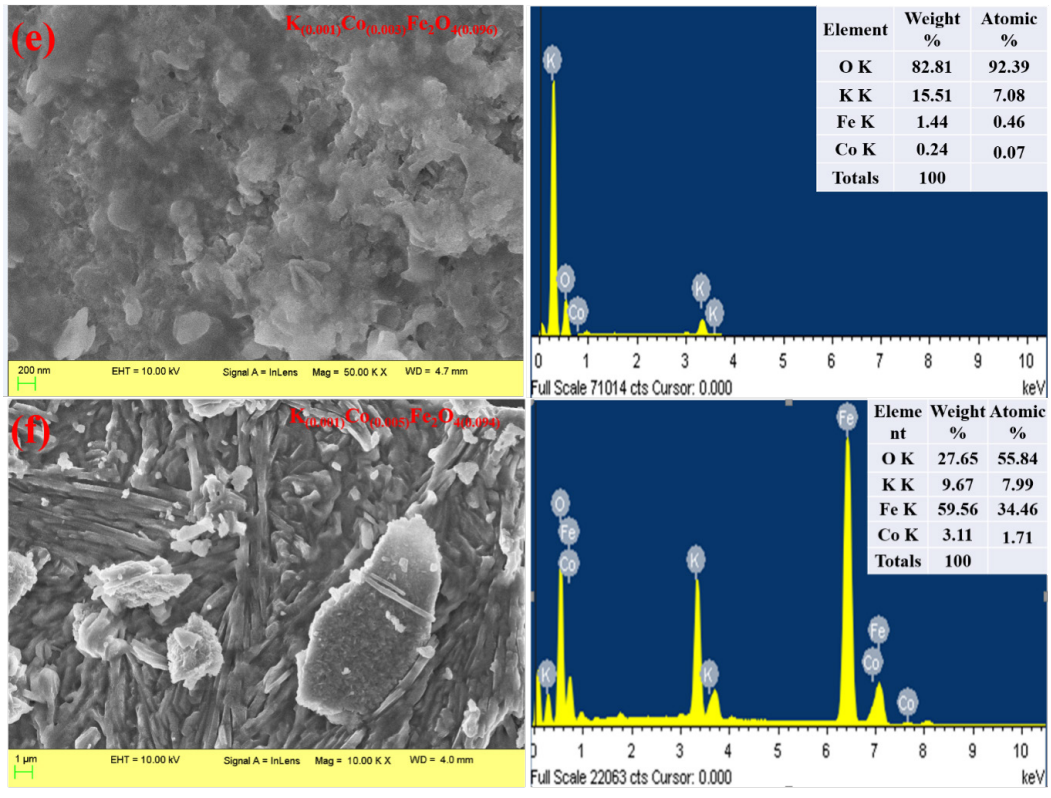

3.3. TEM Results

The average size of the doped NPs was computed using TEM analysis. The morphological results were well-aligned with the SEM outcomes. The TEM results showed that the average particle size ranges between 60–68 nm for $Na_{(0.001)}Co_{(0.001)}Fe_2O_{4(0.098)}$, $Na_{(0.001)}Co_{(0.003)}Fe_2O_{4(0.096)}$, and $Na_{(0.001)}Co_{(0.005)}Fe_2O_{4(0.094)}$ (**Fig. 3 (a–c)**). Similarly, the average particle size range for $K_{(0.001)}Co_{(0.001)}Fe_2O_{4(0.098)}$, $K_{(0.001)}Co_{(0.003)}Fe_2O_{4(0.096)}$, and $K_{(0.001)}Co_{(0.005)}Fe_2O_{4(0.094)}$ falls in the range between 26–66 nm (**Fig. 3 (d–f)**). The discrepancy between particle sizes measured from XRD patterns and those observed in TEM images can be attributed to the different aspects each technique evaluates. XRD analysis estimates crystallite size using the Scherrer equation, which reflects the dimensions of a single coherent, diffracting domain. In contrast, a single particle observed in TEM may consist of multiple crystallites due to agglomeration or polycrystalline structure (Hassanzadeh-Tabrizi, 2023; Holder & Schaak, 2019; Pelka et al., 2024). Therefore, particle size—representing the overall physical dimensions of aggregated crystallites—is typically larger than the crystallite size (Mongkolsuttirat & Buajarern, 2021; Sabur & Gafur, 2024). This difference accounts for the variation observed between crystallite and particle sizes in the Na/K/$CoFe_2O_4$ nanoparticles. On comparing particle size in cobalt ferrites because of doping by Na and K, there is a decrease in particle size when cobalt ferrites are doped by K. This can be attributed to the reason that K^+ ions are much larger, causing lattice strain when incorporated into spinel cobalt ferrites. This strain inhibits crystal growth, leading to smaller and less regular particles (Desoky et al., 2022). The comparison of properties based on the outcomes is also tabulated in **Table 2**.

Table 2. Comparison of properties of Na and K-doped cobalt ferrite samples

Property	Na-doped $CoFe_2O_4$	K-doped $CoFe_2O_4$
Particle Size	Larger	Smaller
Shape	Spherical and Slightly Faceted	Irregular or rough
Surface Roughness	Smoother	Rougher
Lattice strain	Low	High
Aggregation	Less	More
Defects and vacancies	Less	More

Figure 3. TEM micrographs and average particle size histograms of various Na and K-doped cobalt ferrite (a–f) samples

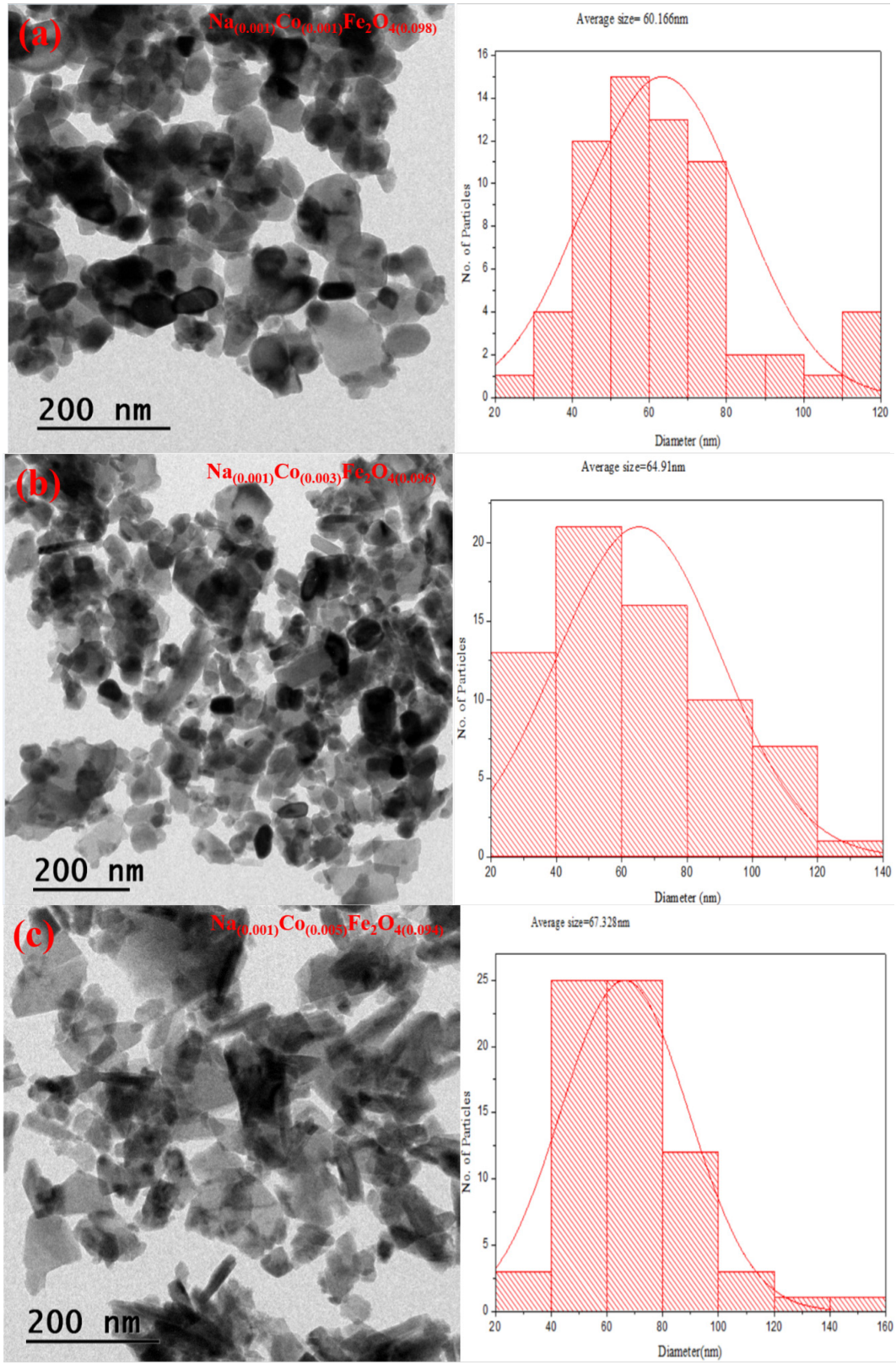

 https://doi.org/10.37819/nanofab.10.2069

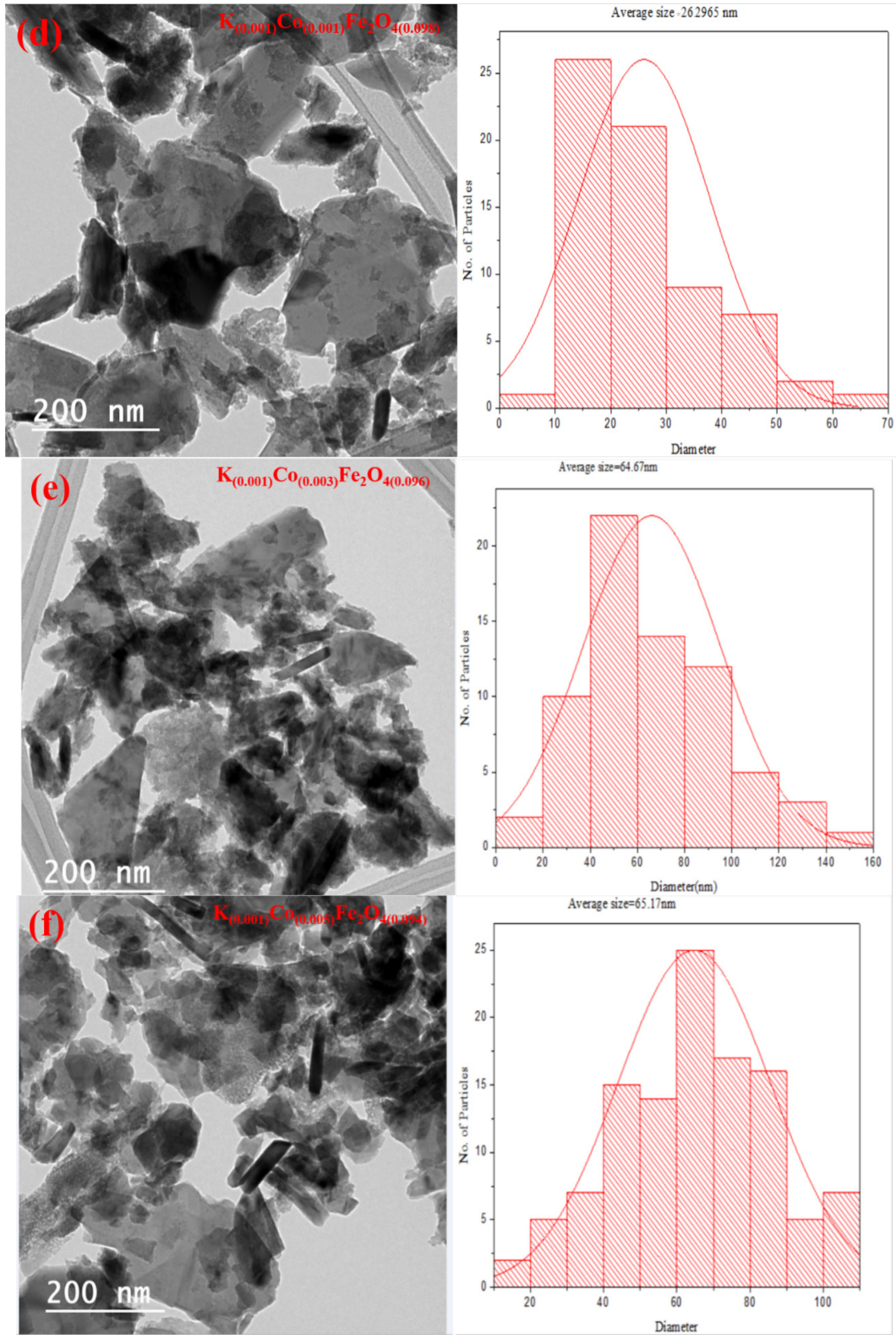

3.4. UV-Vis Results

The UV-Vis absorbance spectra were utilized to investigate the optical properties of synthesized pure and doped ferrite samples in the wavelength range of 200–800 nm, as shown in **Fig. 4**. This has been reported in the literature that cobalt ferrites show peak between 330 nm to 550 nm for UV studies (Mushtaq et al., 2017). The absorbance value for $Na_{(0.001)}Co_{(0.001)}Fe_2O_{4(0.098)}$ increases at 258 nm, and further, the absorbance peak is observed around 333 nm, 342 nm, and is steady till 522 nm, and then an absorption curve is seen at 640 nm. The graph for $Na_{(0.001)}Co_{(0.003)}Fe_2O_{4(0.096)}$ increases at 259 nm, and the range in between maximum absorption is from 335 nm to 383 473 nm, and a slight peak at around 541 and 646 nm. The next graph for $Na_{(0.001)}Co_{(0.005)}Fe_2O_{4(0.094)}$ shows a steady increase in absorbance and a peak at 259 nm, and further a peak at 343 nm, 490 nm, around 556 nm, and a slight curve at around 690 to 696 nm. As the concentration of cobalt is increased in $Na_{(0.001)}Co_{(0.003)}Fe_2O_{4(0.096)}$ and $Na_{(0.001)}Co_{(0.005)}Fe_2O_{4(0.094)}$, as compared to $Na_{(0.001)}Co_{(0.001)}Fe_2O_{4(0.098)}$, there is a slight increase in the wavelength and this can be attributed to redshift as increasing cobalt content leads to change in the electronic structure (Nithiyanantham et al., 2020; Thakur et al., 2022; Vinosha et al., 2017). The UV spectra for $K_{(0.001)}Co_{(0.001)}Fe_2O_{4(0.098)}$ exhibit an absorption peak at 259 to 261 nm, then there is an increase in absorption intensity, and the maximum steady absorption is from 439 nm to 489 nm. The absorption continues till 580 nm. For $K_{(0.001)}Co_{(0.003)}Fe_2O_{4(0.096)}$, maximum absorption is observed from 473 to 566 nm. In the case of $K_{(0.001)}Co_{(0.005)}Fe_2O_{4(0.094)}$, the first peak is observed around 266 nm, and the maximum absorption is around 497 to 568 nm. The increase in maximum absorption wavelength for NPs with an increase in the concentration of cobalt can be attributed to redshift and electronic changes, and lattice distortion (Malik et al., 2021; Ullah et al., 2021).

The band gap evaluation for the cobalt ferrite samples was calculated using Tauc's relation (equation 3)

$$(\alpha h\nu)^n = B(h\nu - E_g) \quad (3)$$

where (α) is the absorption coefficient, E_g is the optical band gap (in eV), B is Tauc's constant, and n is the value that depends on the type of transition, here $n = 1/2$, i.e., it is a direct allowed transition. The values obtained for $Na_{(0.001)}Co_{(0.001)}Fe_2O_{4(0.098)}$, $Na_{(0.001)}Co_{(0.003)}Fe_2O_{4(0.096)}$, and $Na_{(0.001)}Co_{(0.005)}Fe_2O_{4(0.094)}$ is 1.65, 1.61, and 1.50 eV, respectively (**Fig. 4 (b)**). Similarly, the band gap for $K_{(0.001)}Co_{(0.001)}Fe_2O_{4(0.098)}$, $K_{(0.001)}Co_{(0.003)}Fe_2O_{4(0.096)}$, and $K_{(0.001)}Co_{(0.005)}Fe_2O_{4(0.094)}$ have been 1.41, 1.12, and 1.05 eV respectively (**Fig. 4 (d)**). The study by Kamakshi et al. (2024) also confirmed the band gap values of doped ferrite samples near 1.6 eV.

Figure 4. UV-Vis spectra and band gap of Na and K-doped cobalt ferrite (a–d) samples

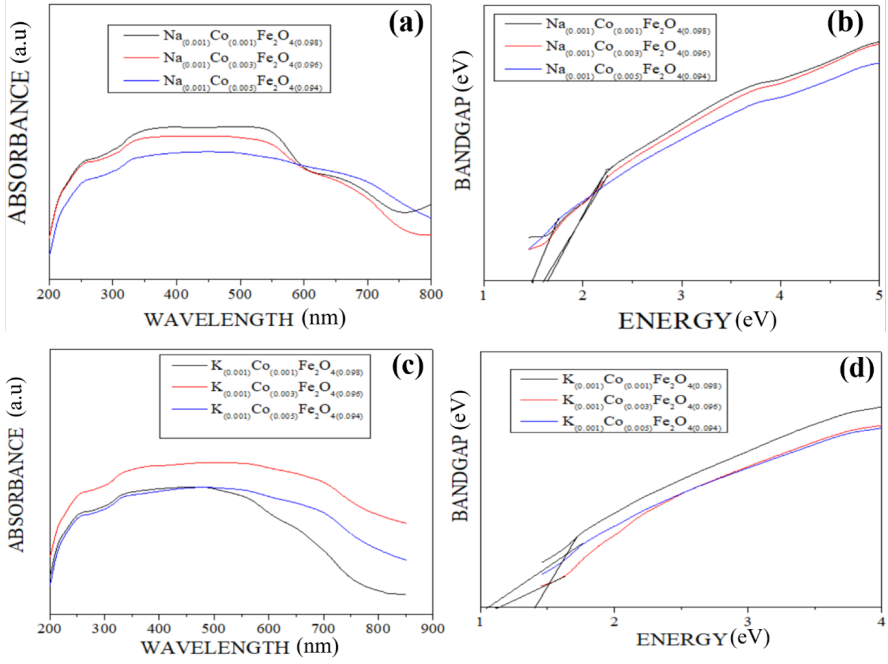

 https://doi.org/10.37819/nanofab.10.2069

3.5. Photocatalytic Degradation Results

Photocatalytic activity is the potential of a material to commence a chemical reaction in the presence of light (Vasiljevic et al., 2020). The photocatalytic activity of the samples has been studied by photochemical degradation of MO and MB, which are industrial pollutants. UV-Visible spectra have been recorded from 400 to 800 nm at an interval of 10 min for a total of 90 min. The characteristic peaks for both dyes are at 468 and 668 nm, respectively. The control experiments were carried out in the dark i.e. without light (Dark adsorption control) in which a 100 ml solution of dyes MO and MB (both taken separately) were both subjected to NPs in dark and it was observed that there is no photodegradation, only a bit drop in concentration which can be attributed to the fact that there is adsorption of dye molecules on the surface of the catalyst (Gogoi et al., 2021; Tabassum et al., 2024). Another experiment was carried out in which catalysts, i.e., nanoparticles, were not used and involved light-induced decomposition control (Speight, 2018). Both dyes were subjected to light without the catalyst, and the result was no degradation. **Table 3** summarizes the photocatalytic activity with control experiments. There is minimal photocatalytic activity without a catalyst, and the literature also confirms less degradation of dyes in the absence of light (Jelokhani et al., 2020; Sanchez-Lievanos et al., 2024). % degradation of dyes with K-doped photocatalyst without light is presented in **Fig. 5**.

Table 3. Details of Control Experiments

Control Experiment	NPs Used as Catalysts	UV-Light Used	Results
Dark adsorption control (without light)	K-$CoFe_2O_4$ was used	No	Very less degradation of both the dyes
Light-induced decomposition Control (without catalyst)	None	Yes	Minimal photodegradation of both the dyes

Figure 5. % degradation of 25 mg dosage of K-doped cobalt ferrite with MB (a) and MO (b) in the dark

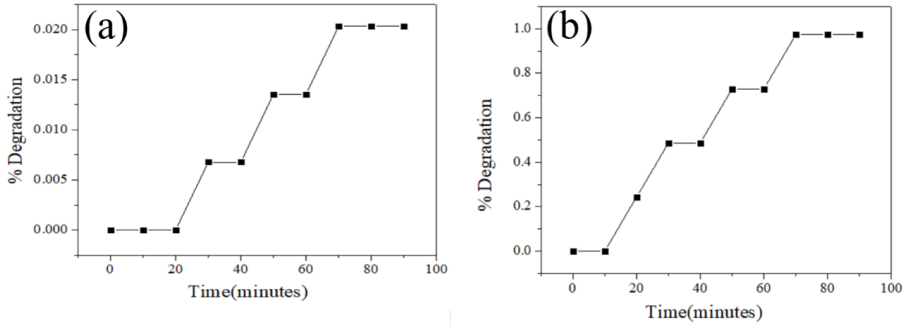

The percentage degradation of the dyes has been discussed in **Fig. 6** and **Fig. 7**. The maximum photocatalytic activity shown by Na and K-doped $CoFe_2O_4$ NPs was at 25 mg dosage for both MO and MB dyes. The formula used for evaluating the degradation (%) of dye is given in equation (4).

$$\% \text{ Degradation} = (A_0 - A_t)/A_0 * 100 \quad (4)$$

where A_0 is the absorbance of a pure solution of dye, while A_t is the absorbance of the reaction mixture at any time *t*.

From **Table 4**, the photocatalytic activity of samples is higher in the case of K-doped cobalt ferrite NPs as compared to K-doped cobalt ferrite NPs. This can be attributed to the fact that K-doped NPs have smaller sizes and band gaps as compared to Na-doped NPs, as a result, more surface area, more oxygen vacancies, and better charge separation ability which makes them more efficient for photocatalytic degradation of organic pollutants like dyes (Khatamian et al., 2024). Also, an increase in the quantity of the NPs enhances the photocatalytic activity. The photocatalytic activity is maximum when the quantity is maximum, i.e., 25 mg, and minimum when the quantity is least, i.e., 5 mg, for Na-doped cobalt ferrites as well as for K-doped cobalt ferrite NPs. The reason behind this is that if the quantity of photocatalyst added is well below the

optimal value, it readily degrades the substance due to more availability of free radicals, resulting in the rate of increase of the reaction (Dhiman et al., 2019).

Among many factors that affect photocatalytic activity, one of the most prominent is the effect of doping. The action of the photocatalyst is based on Langmuir-Hinshelwood theory (Saeed et al., 2018). Whenever there is light irradiation on the surface of a photocatalyst (PC), electrons are excited from the valence band to the conduction band if the energy of the incident radiation is greater than the band gap. Accordingly, there is a generation of electrons and holes, electrons are excited to the conduction band while holes are created in the valence band as shown in equations (5–7).

$$PC + light \rightarrow e^-_{CB} + h^+_{VB} \quad (5)$$

$$h^+_{VB} \rightarrow \text{Valence band} \quad (6)$$

$$e^-_{CB} \rightarrow \text{Conduction band} \quad (7)$$

In the Conduction band the irradiated electron from the surface combines with oxygen on the surface to form superoxide ions. These ions in turn combine with water to form hydrogen peroxide, which generates hydroxide radicals to react with dye molecules to degrade it (equation (8–9)).

$$O_2 + e^-_{CB} \rightarrow O_2^- \quad (8)$$

$$H_2O + O_2^- \rightarrow H_2O_2 \rightarrow 2OH \quad (9)$$

Meanwhile, in the valence band, there are holes where hydroxyl radicals (OH^-) are generated because of the interaction of the photogenerated holes with water molecules, the OH^- radicals thus generated react with dye molecules and thus a chain of free radicals is formed by the consumption of oxygen, and organic pollutants are converted into degraded products (equations (10–11)) (Aroob et al., 2023).

$$h^+_{VB} + H_2O \rightarrow OH + H^+ \quad (10)$$

$$Dye + OH \rightarrow H_2O + CO_2 \quad (11)$$

Figure 6. % degradation of MB (a–c) and MO (d–f) at different dosages (5, 15 & 25 mg) of Na-doped cobalt ferrite samples

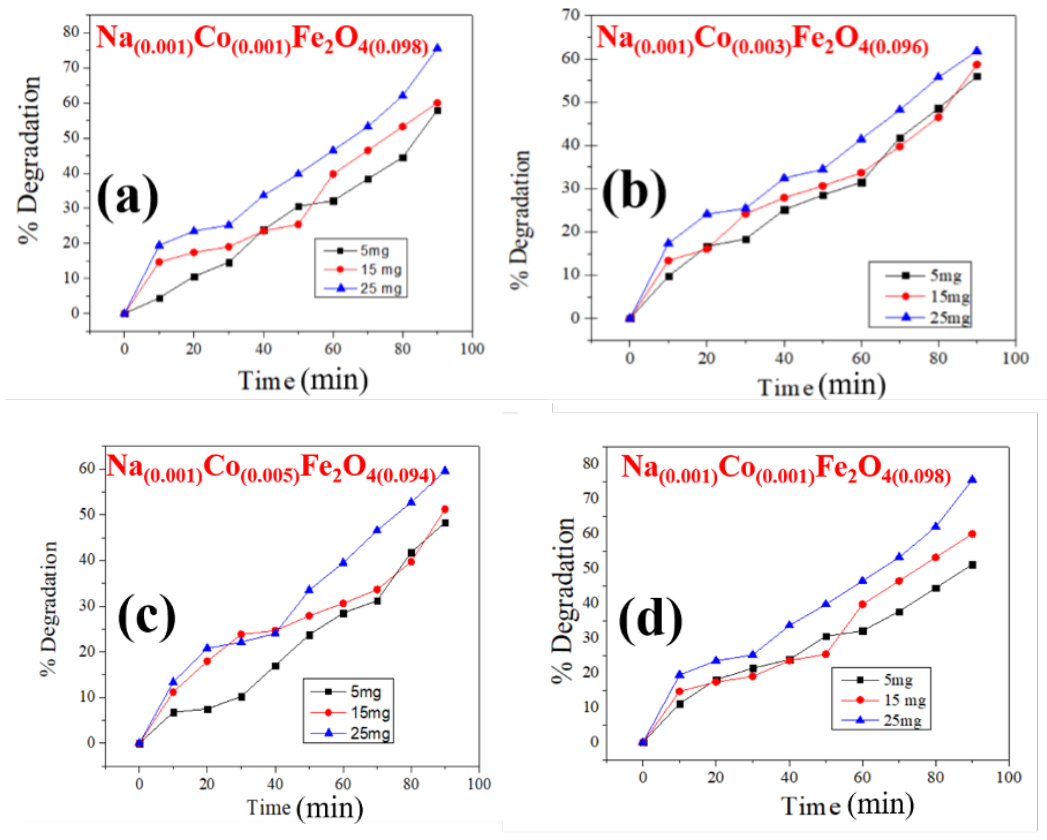

 https://doi.org/10.37819/nanofab.10.2069

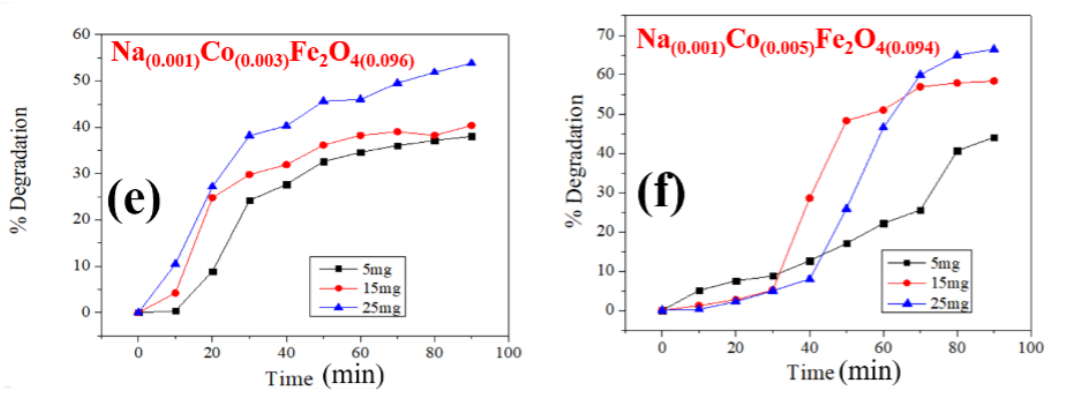

Figure 7. % degradation of MB (a–c) and MO (d–f) at different dosages (5, 15 & 25 mg) of K-doped cobalt ferrite samples

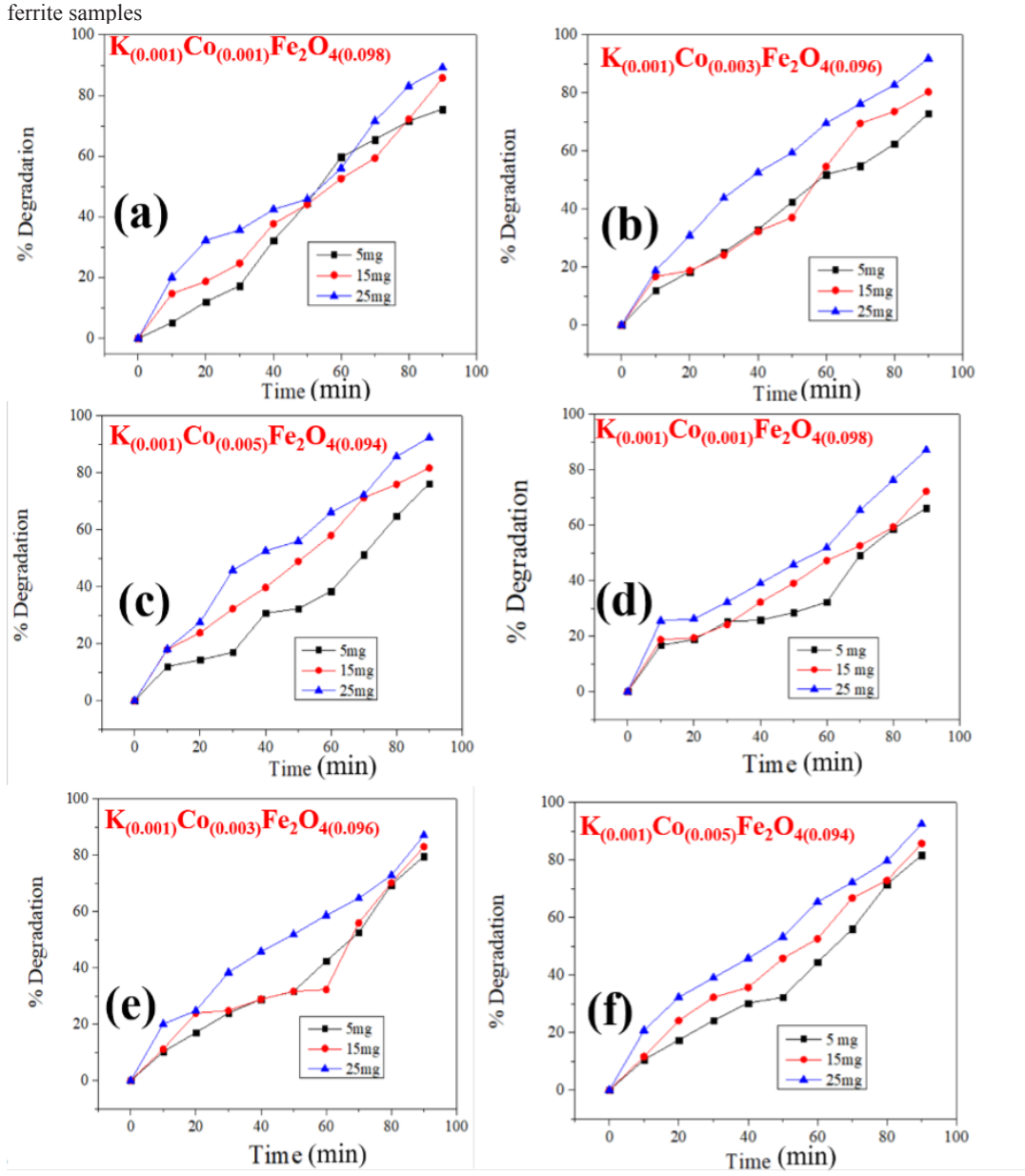

Table 4. % degradation of Na and K-doped cobalt ferrite samples

Samples	Dosage (mg)	Time (min)	% Degradation of MO	% Degradation of MB
$Na_{(0.001)}Co_{(0.001)}Fe_2O_{4(0.098)}$	5	90	51.25	55.99
	15	90	60.05	60.02
	25	90	75.62	75.60
$Na_{(0.001)}Co_{(0.003)}Fe_2O_{4(0.096)}$	5	90	40.25	55.99
	15	90	40.38	58.70
	25	90	53.81	61.81
$Na_{(0.001)}Co_{(0.005)}Fe_2O_{4(0.094)}$	5	90	44.03	48.34
	15	90	58.37	51.25
	25	90	66.41	59.65
$K_{(0.001)}Co_{(0.001)}Fe_2O_{4(0.098)}$	5	90	66.14	75.49
	15	90	72.24	85.78
	25	90	87.13	89.23
$K_{(0.001)}Co_{(0.003)}Fe_2O_{4(0.096)}$	5	90	79.68	72.91
	15	90	83.07	80.36
	25	90	87.10	91.87
$K_{(0.001)}Co_{(0.005)}Fe_2O_{4(0.094)}$	5	90	81.72	76.30
	15	90	85.78	81.72
	25	90	92.55	92.41

3.6. Antioxidant Results

The DPPH assay method was utilized to study the antioxidant activity of a substance, as it is one of the most prevalent methods. Its principle is based on the method of stabilizing DPPH free radicals by antioxidants whose activity can be assessed by the decolorization of DPPH in methanol solution (Rubab et al., 2022; Škrovánková et al., 2012; Sohel Rana et al., 2024). Antioxidants are counterbalancing species that curtail the harm caused by various oxidative processes to living cells; they donate electrons to free radicals, thus making them harmless (Baliyan et al., 2022a). DPPH, i.e., 1,1-diphenyl-2-picrylhydrazyl, is a stable free radical with an odd electron on nitrogen. It acts as a scavenger for antioxidants, which donate electrons to free radicals, making them harmless by causing neutralization. The stability of the radicals is due to the steric crowding on the divalent nitrogen atom carrying an odd electron and the pulling-pushing effect of the diphenyl amino group, which acts as an electron donor, and the picryl group, which is an electron acceptor (Gulcin & Alwasel, 2023). Thus, it is a stabilized violet-coloured radical that absorbs at 517 nm. In the present study, K-doped $CoFe_2O_4$ NPs exhibited excellent antioxidant properties, which makes them outstanding antioxidants. This is attributed to the increased surface-to-volume ratio and increased surface area that leads to effective binding of the substrates (Kanagesan et al., 2016; Pozzi et al., 2024). The antioxidant activity increases with the increase in concentration, and this may be attributed to the transfer of free electrons from the oxygen atom of the doped samples to the nitrogen free radical in the DPPH molecule. There is a significant difference in the antioxidant activity of Na and K-doped cobalt ferrite NPs at different concentrations, as tabulated in **Table 5**, and the results are evaluated using equation (12):

$$\% \text{ Scavenging Activity} = \frac{Abs_{\text{control}} - Abs_{\text{sample}}}{Abs_{\text{control}}} \times 100 \quad (12)$$

Each sample was analysed in triplicate for its antioxidant scavenging activity. The average values have been replicated, as can be seen in **Table 5**. However, when antioxidant activity was compared with that of ascorbic acid, it was found to be lower (**Fig. 8**). **Fig. 8** indicated the relative activity of Na and K-$CoFe_2O_4$ NPs with ascorbic acid. The various reasons attributed to the increase in antioxidant

activity include an increase in oxygen vacancies, an increase in surface-to-volume ratio, a better penetration effect due to a decrease in particle size, creation of surface electrons, which increase antioxidant activity (Robkhob et al., 2020). It is also observed that the antioxidant activity of K-cobalt ferrites is more than the antioxidant activity of Na-doped cobalt ferrite NPs which could be due to the better penetration effect as there is a decrease in crystallite size of K-doped NPs.

Table 5. Scavenging activity of Na and K-doped cobalt ferrite samples

Samples	Absorbance of Control	Absorbance of Samples	% Scavenging
$Na_{(0.001)}Co_{(0.001)}Fe_2O_{4(0.098)}$	1.589	0.409	74.26 ± 0.21
$Na_{(0.001)}Co_{(0.003)}Fe_2O_{4(0.096)}$	1.589	0.395	75.14 ± 0.29
$Na_{(0.001)}Co_{(0.005)}Fe_2O_{4(0.094)}$	1.589	0.280	82.37 ± 0.31
$K_{(0.001)}Co_{(0.001)}Fe_2O_{4(0.098)}$	1.589	0.090	94.33 ± 0.40
$K_{(0.001)}Co_{(0.003)}Fe_2O_{4(0.096)}$	1.589	0.059	96.28 ± 0.36
$K_{(0.001)}Co_{(0.005)}Fe_2O_{4(0.094)}$	1.589	0.050	96.85 ± 0.25
Ascorbic acid	1.589	0.005	99.68 ± 0.19

Figure 8. Scavenging activity of Na and K-doped cobalt ferrite samples

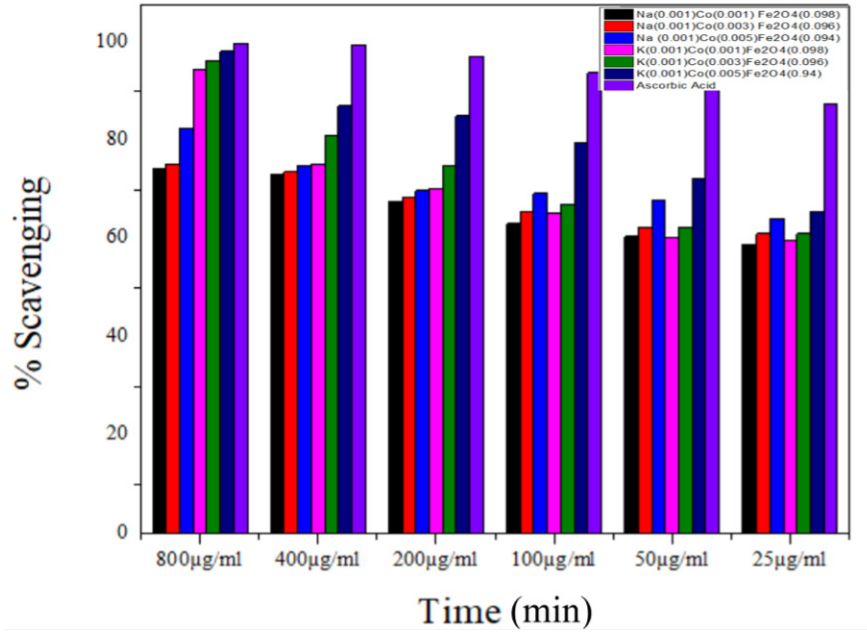

3.6.1 Mechanism of Antioxidant Activity

The DPPH assay method is one of the most prevalent methods to study the antioxidant activity of a substance. Its principle is based on the method of forage of DPPH by antioxidants, and the antioxidant activity of a substance or species can be assessed by decolourisation of DPPH methanolic solution. Antioxidants are counterbalancing species that curtail the harm caused by various oxidative processes to living cells; they donate electrons to free radicals, thus making them harmless. DPPH, i.e., 1,1-diphenyl-2-picrylhydrazyl, is a stable free radical with an odd electron on nitrogen. It acts as a scavenger for antioxidants, as antioxidants donate electrons to free radicals, making them harmless by causing neutralization. The stability of the radicals is due to the steric crowding on the divalent nitrogen atom carrying an odd electron and the pulling-pushing effect of the diphenyl amino group, which acts as an electron donor, and the picryl group, which is an electron acceptor. In other words, its structures are resonance stabilized. Thus, it is a

stabilised violet coloured radical which absorbs at 517 nm. DPPH has a strong affinity for free radicals like $OH^{\cdot}$, $NO^{\cdot}$, $RS^{\cdot}$, $O_2^{\cdot}$. ROS (Reactive Oxygen Species) are molecules and free radicals that originate from molecular oxygen (Kozlov et al., 2024; Moldogazieva et al., 2023). They have both beneficial and harmful characteristics. Oxidative stress is one of the repercussions of their excessive production. Oxygen is highly electronegative and has a tendency to accept electrons, and as a result, it produces ROS like H_2O_2, $OH^{\cdot}$ (Hydroxyl radical) and Superoxide anion radical (O_2^{-}), singlet oxygen, ozone, etc. In the cellular mechanism of homosapiens they are produced as byproducts in oxygen-related mechanisms (Mammarella et al., 2016). In addition to their production as a result of normal metabolic activities, they are also produced as a result of various paraneoplastic and clinical processes (Zhu et al., 2015). The antioxidant activity of NPs involves two mechanisms:

A hydrogen atom transfer (HAT) method in which hydrogen is used for the formation of ROS (Siddeeg et al., 2021). HAT mechanism involves the following steps:

$$OH \cdot (ROS) + \text{Antioxidant (Hydrogen donor)} \rightarrow H_2O + \text{Antioxidant (Oxidised)} \quad (13)$$

$$ROO \cdot (ROS) + \text{Antioxidant (Hydrogen donor)} \rightarrow ROOH + \text{Antioxidant (Oxidised)} \quad (14)$$

$$O_2^{-} + \text{Antioxidant (hydrogen donor)} \rightarrow H_2O_2 + \text{Antioxidant (Oxidised)} \quad (15)$$

A single electron transfer-proton transfer (SET-PT) method, which involves the transference of an electron by an antioxidant (Fragou et al., 2023). SET-PT mechanism involves the following steps:

$$\text{Antioxidant} \rightarrow \text{Antioxidant}^{+} \text{ (Radical cation)} + e^{-} \quad (16)$$

$$\text{Antioxidant}^{+} \rightarrow \text{Antioxidant} + H^{+} \text{ (deprotonation)} \quad (17)$$

$$ROS\ (OH^{\cdot}, ROO^{\cdot}, O_2^{-}) + H^{+} \rightarrow H_2O \text{ or } ROOH \text{ or } H_2O_2 \quad (18)$$

3.6.2 Effect of Doping on the Antioxidant Properties

Doping enhances the antioxidant activity of NPs, as can be seen here, $CoFe_2O_4$ when doped with Na shows antioxidant activity comparable to that of ascorbic acid. The various reasons attributed to the increase in antioxidant activity include an increase in Oxygen vacancies (Hernández-Castillo et al., 2019) effect on lowering of band gap, an increase in surface-to-volume ratio (Mejia-Mendez et al., 2024), a better penetration effect due to a decrease in particle size creation of surface electrons which increases antioxidant activity (Robkhob et al., 2020). Here we can see that the antioxidant activity of K-doped Cobalt ferrites is more than the antioxidant activity of Na-doped cobalt ferrite NPs and the reason may be due to the better penetration effect, as there is a decrease in crystallite size of K-doped NPs. Further, due to smaller crystallite size in case of K-doped NPs, surface-to-surface interaction and as a result reactivity for free radicals is increased, leading to better antioxidant activity. Also, Potassium creates more lattice strain as the ionic size of K^{+} (1.38Å) is greater than that of Na^{+} (1.02Å) and as a result produces more Oxygen Vacancies, which are detrimental for ROS scavenging (Sundram et al., 2022). Another noticeable trend is that there is a slight increase in antioxidant activity as we increase the concentration of Cobalt, keeping the overall and dopant concentration the same. As can be seen from the XRD data of **Table 1**, as we increase the concentration of Cobalt, there is increase in Crystallite size relatively in Sodium and Potassium doped nanoparticles but still there is slight increase in antioxidant activity, this can be attributed to the fact that slight increase in crystallite size which might decrease antioxidant activity is compensated by increase in oxygen vacancies and increase in magnetic properties, which lead to increase in electron transfer and hence improve the antioxidant activity. Further, there is also an increase in lattice strain with an increase in anti-oxidant activity, which facilitates ROS activity, thus compensating increase in particle size and decrease in surface area (Milutinović et al., 2024).

4. CONCLUSIONS

In conclusion, it is clear from the present study that doping affects the photocatalytic and antioxidant properties of cobalt ferrite NPs due to alteration in surface, change in band gap, interface properties, and change in size. These factors influence the penetration ability of the NPs to act as antioxidants. Here, sodium and potassium act as dopants having different properties due to differences in ionic radii. As is clear from the studies, if we compare the photocatalytic properties

of sodium and potassium-doped cobalt ferrite NPs, potassium-doped NPs show relatively more degradation activity. Small particle size and more lattice strain have been instrumental in enhancing the photocatalytic and antioxidant abilities of potassium cobalt ferrite NPs in comparison to sodium-doped cobalt ferrite NPs. Moreover, since the concentration of dopant has been kept the same, a change in the concentration of cobalt will automatically change the concentration of iron oxide, as the overall concentration must be the same. Thus, optimum doping is one of the most convenient ways to augment photocatalytic and antioxidant applications of NPs. Alkali metals can be used as good dopants in optimum concentrations.

One of the most practical applications of the enhanced photocatalytic activity of nanoparticles is in water remediation, as previously discussed. This approach is cost-effective, particularly because sodium (Na) and potassium (K) are abundant, inexpensive, and less toxic, making them suitable candidates for environmental remediation, including air purification. Doping metal ferrites and oxides with these elements has also been shown to reduce cytotoxicity. Another promising application lies in regulating oxidative stress by acting as reactive oxygen species (ROS) scavengers, thereby exhibiting antioxidant properties. This function can aid in the prevention of various diseases. Additionally, their antioxidant capabilities can be leveraged to extend the shelf life of perishable products such as food, pharmaceuticals, and cosmetics.

Overall, the improved photocatalytic and antioxidant properties of these nanoparticles offer broad and impactful practical applications across multiple fields.

Declarations of Competing Interest

The authors declare no competing interests.

Acknowledgments

The authors are thankful to the Sophisticated Analytical Instrumentation Facility (SAIF), Panjab University (Punjab), and Sprint Testing Solutions, Mumbai (Maharashtra) for the assistance in the characterization of samples.

References

Abd El-Salam, A. R., Rady, K. E., ELFadaly, E. A., & Aly, M. H. (2023). Enhanced Structural and Morphological Properties of Doped Cobalt Zinc Ferrite. *Journal of Nanotechnology and Nanomaterials*, *4*(2), 89–93.

Albalah, M. A., Alsabah, Y. A., & Mustafa, D. E. (2020). Characteristics of co-precipitation synthesized cobalt nanoferrites and their potential in industrial wastewater treatment. *SN Applied Sciences*, *2*(5), 804. https://doi.org/10.1007/s42452-020-2586-6

Amani, H., Habibey, R., Hajmiresmail, S. J., Latifi, S., Pazoki-Toroudi, H., & Akhavan, O. (2017). Antioxidant nanomaterials in advanced diagnoses and treatments of ischemia reperfusion injuries. *Journal of Materials Chemistry B*, *5*(48), 9452–9476.

Aroob, S., Carabineiro, S. A., Taj, M. B., Bibi, I., Raheel, A., Javed, T., Yahya, R., Alelwani, W., Verpoort, F., & Kamwilaisak, K. (2023). Green synthesis and photocatalytic dye degradation activity of CuO nanoparticles. *Catalysts*, *13*(3), 502.

Baliyan, S., Mukherjee, R., Priyadarshini, A., Vibhuti, A., Gupta, A., Pandey, R. P., & Chang, C.-M. (2022a). Determination of antioxidants by DPPH radical scavenging activity and quantitative phytochemical analysis of Ficus religiosa. *Molecules*, *27*(4), 1326.

Barkat, F., Afzal, M., Khan, B. S., Saeed, A., Bashir, M., Mukhtar, A., Mehmood, T., & Wu, K. (2022). Formation mechanism and lattice parameter investigation for copper-substituted cobalt ferrites from Zingiber officinale and Elettaria cardamom seed extracts using biogenic route. *Materials*, *15*(13), 4374.

Bhardwaj, B., Tiwari, P. R., Bharati, K., Singh, R. P., Yadav, A. C., Singh, K. A., Yadav, B. C., & Kumar, S. (2024). Synthesis, characterisation and application of ca-doped CoFe2O4 nanoparticles in humidity sensing. *Advances in Applied Ceramics*, *123*(7–8), 130–141. https://doi.org/10.1177/17436753241308031

Ceballos-Sanchez, O., Navarro-López, D. E., Mejía-Méndez, J. L., Sanchez-Ante, G., Rodríguez-González, V., Sánchez-López, A. L., Sanchez-Martinez, A., Duron-Torres, S. M., Juarez-Moreno, K., & Tiwari, N. (2024). Enhancing antioxidant properties of CeO_2 nanoparticles with Nd^{3+} doping: Structural, biological, and machine learning insights. *Biomaterials Science*, *12*(8), 2108–2120.

Desoky, W. M., Gutierrez, J., El-Bana, M. S., & Elmoslami, T. A. (2022). Exploring the impact of nickel doping on the structure and

low-temperature magnetic features of cobalt nano-spinel ferrite. *Applied Physics A*, *128*(9), 846. https://doi.org/10.1007/s00339-022-05977-0

Dhiman, M., Chudasama, B., Kumar, V., Tikoo, K. B., & Singhal, S. (2019). Augmenting the photocatalytic performance of cobalt ferrite via change in structural and optical properties with the introduction of different rare earth metal ions. *Ceramics International*, *45*(3), 3698–3709.

Dippong, T., Levei, E. A., Petean, I., Deac, I. G., Mereu, R. A., & Cadar, O. (2023). Screening of Mono-, Di-and Trivalent Cationic Dopants for the Enhancement of Thermal Behavior, Kinetics, Structural, Morphological, Surface and Magnetic Properties of $CoFe_2O_4$-SiO_2 Nanocomposites. *International Journal of Molecular Sciences*, *24*(11), 9703.

do Carmo Dias, G., de Souza, N. C. S., de Souza, E. I. P., Puiatti, G. A., & Moreira, R. P. L. (2024). Enhanced degradation of Direct Red 80 dye via Fenton-like process mediated by cobalt ferrite: Generated superoxide radicals and singlet oxygen. *Environmental Science and Pollution Research*, *31*(19), 28025–28039. https://doi.org/10.1007/s11356-024-32976-w

Elansary, M., Belaiche, M., Oulhakem, O., Alaoui, K. B., Lemine, O. M., Mouhib, Y., Iffer, E., Salameh, B., & Alsmadi, A. M. (2024). In-depth study of the photocatalytic performance of novel magnetic catalysts for efficient photocatalytic degradation of the dye orange G. *Materials Research Bulletin*, *170*, 112598.

Fragou, F., Theofanous, A., Deligiannakis, Y., & Louloudi, M. (2023). Nanoantioxidant Materials: Nanoengineering Inspired by Nature. *Micromachines*, *14*(2), Article 2. https://doi.org/10.3390/mi14020383

Girija, R., Mary, S., Balakrishnan, G., Mariappan, S. M., Hamdy, M. S., & Shkir, Mohd. (2022). Noticeably Improved Visible Light Photocatalytic Activity of TiO_2 Nanoparticles through co-Doping of Activated Charcoal and Fe Towards Methylene Blue Degradation. *ChemistrySelect*, *7*(5), e202103614. https://doi.org/10.1002/slct.202103614

Gogoi, D., Makkar, P., & Ghosh, N. N. (2021). Solar Light-Irradiated Photocatalytic Degradation of Model Dyes and Industrial Dyes by a Magnetic $CoFe_2O_4$–gC_3N_4 S-Scheme Heterojunction Photocatalyst. *ACS Omega*, *6*(7), 4831–4841. https://doi.org/10.1021/acsomega.0c05809

Gulcin, İ., & Alwasel, S. H. (2023). DPPH radical scavenging assay. *Processes*, *11*(8), 2248.

Hameed, S., Waqas, M., Zahid, S., Gul, S., Shawky, A. M., Alatawi, N. S., Shehzad, R. A., Bhatti, I. A., Ayub, K., & Iqbal, J. (2023). Quantum Chemical Approach of Hexaammine $(NH_3)_6$ complexant with alkali and alkaline earth metals for their potential use as NLO materials. *Journal of Molecular Graphics and Modelling*, *123*, 108505.

Harrington, G. F., Kim, S., Sasaki, K., Tuller, H. L., & Grieshammer, S. (2021). Strain-modified ionic conductivity in rare-earth substituted ceria: Effects of migration direction, barriers, and defect-interactions. *Journal of Materials Chemistry A*, *9*(13), 8630–8643.

Hassanzadeh-Tabrizi, S. A. (2023). Precise calculation of crystallite size of nanomaterials: A review. *Journal of Alloys and Compounds*, *968*, 171914. https://doi.org/10.1016/j.jallcom.2023.171914

Hernández-Castillo, Y., García-Hernández, M., López-Marure, A., Luna-Domínguez, J. H., López-Camacho, P. Y., & Morales-Ramírez, Á. de J. (2019). Antioxidant activity of cerium oxide as a function of europium doped content. *Ceramics International*, *45*(2, Part A), 2303–2308. https://doi.org/10.1016/j.ceramint.2018.10.145

Holder, C. F., & Schaak, R. E. (2019). Tutorial on Powder X-ray Diffraction for Characterizing Nanoscale Materials. *ACS Nano*, *13*(7), 7359–7365. https://doi.org/10.1021/acsnano.9b05157

Hossain, M. S., Alam, Md. B., Shahjahan, M., Begum, Most. H. A., Hossain, Md. M., Islam, S., Khatun, N., Hossain, M., Alam, M. S., & Al-Mamun, Md. (2018). Synthesis, structural investigation, dielectric and magnetic properties of Zn^{2+}-doped cobalt ferrite by the sol–gel technique. *Journal of Advanced Dielectrics*, *08*(04), 1850030. https://doi.org/10.1142/S2010135X18500303

Houshiar, M., Zebhi, F., Razi, Z. J., Alidoust, A., & Askari, Z. (2014). Synthesis of cobalt ferrite ($CoFe_2O_4$) nanoparticles using combustion, coprecipitation, and precipitation methods: A comparison study of size, structural, and magnetic properties. *Journal of Magnetism and Magnetic Materials*, *371*, 43–48.

Jelokhani, F., Sheibani, S., & Ataie, A. (2020). Adsorption and photocatalytic characteristics of cobalt ferrite-reduced graphene oxide and cobalt ferrite-carbon nanotube nanocomposites.

Journal of Photochemistry and Photobiology A: Chemistry, *403*, 112867. https://doi.org/10.1016/j.jphotochem.2020.112867

Jhala, I. G., Maru, A., Hathiya, L., Desai, H. B., Shah, N. A., Solanki, P. S., Tanna, A. R., & Joshi, H. H. (2024). Structural, magnetic and electrical properties of gadolinium doped cobalt ferrite nanoparticles: Role of Gd doping level. *Nano-Structures & Nano-Objects*, *40*, 101327. https://doi.org/10.1016/j.nanoso.2024.101327

Kalia, S., & Prasad, N. (2023). Overview of properties, applications, and synthesis of 4d-series doped/substituted cobalt ferrite. *Inorganic Chemistry Communications*, *147*, 110201. https://doi.org/10.1016/j.inoche.2022.110201

Kamakshi, T., Sundari, G. S., Ramachandrarao, M. V., & Jyothsna, A. N. (2024). A novel nickel-doped photoactive nanocomposite materials for the application of wastewater treatment. *Inorganic Chemistry Communications*, *160*, 111945. https://doi.org/10.1016/j.inoche.2023.111945

Kanagesan, S., Hashim, M., AB Aziz, S., Ismail, I., Tamilselvan, S., Alitheen, N. B., Swamy, M. K., & Purna Chandra Rao, B. (2016). Evaluation of antioxidant and cytotoxicity activities of copper ferrite ($CuFe_2O_4$) and zinc ferrite ($ZnFe_2O_4$) nanoparticles synthesized by sol-gel self-combustion method. *Applied Sciences*, *6*(9), 184.

Kausar, A., Sattar, A., Xu, C., Zhang, S., Kang, Z., & Zhang, Y. (2021). Advent of alkali metal doping: A roadmap for the evolution of perovskite solar cells. *Chemical Society Reviews*, *50*(4), 2696–2736.

Kaushal, S., Thakur, N., & Kumar, K. (2024). Investigation of the efficacy of Zn/Ce–CuO nanoparticles for enhanced photocatalytic, antibacterial, and antioxidant activities. *Environmental Science and Pollution Research*. https://doi.org/10.1007/s11356-024-34180-2

Khalil, I., Yehye, W. A., Etxeberria, A. E., Alhadi, A. A., Dezfooli, S. M., Julkapli, N. B. M., Basirun, W. J., & Seyfoddin, A. (2019). Nanoantioxidants: Recent trends in antioxidant delivery applications. *Antioxidants*, *9*(1), 24.

Khanna, L., & Verma, N. K. (2014). Synthesis, characterization and biocompatibility of potassium ferrite nanoparticles. *Journal of Materials Science & Technology*, *30*(1), 30–36.

Khatamian, M., Malekani, M., Fazayeli, M., & Yavari, A. (2024). Improvement of photocatalytic ammonia production of cobalt ferrite nanoparticles utilizing microporous ZSM-5 type ferrisilicate zeolite. *Scientific Reports*, *14*(1), 20301.

Khlyustova, A., Sirotkin, N., Kusova, T., Kraev, A., Titov, V., & Agafonov, A. (2020). Doped TiO_2: The effect of doping elements on photocatalytic activity. *Materials Advances*, *1*(5), 1193–1201.

Kozlov, A. V., Javadov, S., & Sommer, N. (2024). Cellular ROS and Antioxidants: Physiological and Pathological Role. *Antioxidants*, *13*(5), Article 5. https://doi.org/10.3390/antiox13050602

Kumar, R., Kumar, K., Sharma, S., Thakur, N., & Thakur, N. (2023). Multifunctional properties of microwave assisted CuO/Cu_2O-ZnO mixed metal oxide nanocomposites. *Journal of Materials Science: Materials in Electronics*, *34*(16), 1255. https://doi.org/10.1007/s10854-023-10693-3

López-Cano, A. A., Martínez-Aguilar, V., Peña-Juárez, M. G., López-Esparza, R., Delgado-Alvarado, E., Gutiérrez-Castañeda, E. J., Del Angel-Monroy, M., Pérez, E., Herrera-May, A. L., & Gonzalez-Calderon, J. A. (2023). Chemically Modified Nanoparticles for Enhanced Antioxidant and Antimicrobial Properties with Cinnamon Essential Oil. *Antioxidants*, *12*(12), 2057.

López-Ortega, A., Lottini, E., Fernandez, C. de J., & Sangregorio, C. (2015). Exploring the magnetic properties of cobalt-ferrite nanoparticles for the development of a rare-earth-free permanent magnet. *Chemistry of Materials*, *27*(11), 4048–4056.

Malik, M., Chan, K. H., & Azimi, G. (2021). Quantification of nickel, cobalt, and manganese concentration using ultraviolet-visible spectroscopy. *RSC Advances*, *11*(45), 28014–28028.

Mammarella, N., Di Domenico, A., & Fairfield, B. (2016). Aging and the genetic road towards the positivity effect in memory. *Experimental Gerontology*, *82*, 120–124. https://doi.org/10.1016/j.exger.2016.06.011

Manjunatha, K., Chethan, B., Yun Wu, S., Ubaidullah, M., Al-Kahtani, A. A., Dhakal, T., & Jagadeesha, A. V. (2024). Synthesis of Li doped $MgFe_2O_4$ nanoparticles for humidity sensor applications. *Ceramics International*, *50*(15), 27287–27295. https://doi.org/10.1016/j.ceramint.2024.05.026

Mejia-Mendez, J. L., Reza-Zaldívar, E. E., Sanchez-Martinez, A., Ceballos-Sanchez, O., Navarro-López, D. E., Marcelo Lozano, L., Armendariz-Borunda, J., Tiwari, N., Jacobo-Velázquez, D. A., Sanchez-Ante, G.,

& López-Mena, E. R. (2024). Exploring the cytotoxic and antioxidant properties of lanthanide-doped ZnO nanoparticles: A study with machine learning interpretation. *Journal of Nanobiotechnology*, *22*(1), 687. https://doi.org/10.1186/s12951-024-02957-9

Milutinović, A., Lazarević, Z. Ž., Šuljagić, M., & Andjelković, L. (2024). Synthesis-Dependent Structural and Magnetic Properties of Monodomain Cobalt Ferrite Nanoparticles. *Metals*, *14*(7), Article 7. https://doi.org/10.3390/met14070833

M. Matar, S., H. Ramzy, G., Arif, M., M. Maafa, I., Yousef, A., Zouli, N., F. Abouatiaa, A. F., M. Adam, A. S., Y. Qudsieh, I., I. Ali, A., A. Kamoun, E., & Ali, A. (2025). Chemical synthesis of $Nd_xCo_{1-x}Fe_2O_4$ hybrid nanoparticles for permanent magnet applications: Structural, magnetic and electrical properties. *Nanoscale Advances*, *7*(9), 2725–2741. https://doi.org/10.1039/D5NA00197H

Moldogazieva, N. T., Zavadskiy, S. P., Astakhov, D. V., & Terentiev, A. A. (2023). Lipid peroxidation: Reactive carbonyl species, protein/DNA adducts, and signaling switches in oxidative stress and cancer. *Biochemical and Biophysical Research Communications*, *687*, 149167. https://doi.org/10.1016/j.bbrc.2023.149167

Mongkolsuttirat, K., & Buajarern, J. (2021). Uncertainty evaluation of crystallite size measurements of nanoparticle using X-Ray Diffraction analysis (XRD). *Journal of Physics: Conference Series*, *1719*(1), 012054. https://doi.org/10.1088/1742-6596/1719/1/012054

Mozafari, M., & Barbati, M. E. (2024). Oxygen-generating biomaterials for cardiovascular engineering: Unveiling future discoveries. *Drug Discovery Today*, *29*(9), 104135. https://doi.org/10.1016/j.drudis.2024.104135

Mushtaq, M. W., Kanwal, F., Islam, A., Ahmed, K., Haq, Z., Jamil, T., Imran, M., Abbas, S. M., & Huang, Q. (2017). Synthesis and characterisation of doxorubicin-loaded functionalised cobalt ferrite nanoparticles and their in vitro anti-tumour activity under an AC-magnetic field. *Tropical Journal of Pharmaceutical Research*, *16*(7), 1663–1674.

Nithiyanantham, S., Viviliya, S., Anandhan, S., & Mahalakshmi, S. (2020). Synthesis and characterization of cobalt ferrite through Co-precipitation technique. *Lett Appl NanoBioScience*, *10*, 1871–1876.

Nordin, N. A., Farahany, S., Bakar, T. A. A., Hamzah, E., & Ourdjini, A. (2015). Microstructure development, phase reaction characteristics and mechanical properties of a commercial Al–20%Mg_2Si–*x*Ce in situ composite solidified at a slow cooling rate. *Journal of Alloys and Compounds*, *650*, 821–834.

Pelka, R., Nowosielecka, U., Klimza, K., Moszyńska, I., Aidinis, K., Żołnierkiewicz, G., Guskos, A., & Guskos, N. (2024). Nanocrystalline Iron Oxides with Various Average Crystallite Size Investigated Using Magnetic Resonance Method. *Crystals*, *14*(4), Article 4. https://doi.org/10.3390/cryst14040363

Peng, L., Gao, Z., Liang, Y., Guo, X., Zhang, Q., & Cui, D. (2025). Nanoparticle-based drug delivery systems: Opportunities and challenges in the treatment of esophageal squamous cell carcinoma (ESCC). *Nanoscale*, *17*(14), 8270–8288. https://doi.org/10.1039/D4NR05114A

Pozzi, M., Jonak Dutta, S., Kuntze, M., Bading, J., Rüßbült, J. S., Fabig, C., Langfeldt, M., Schulz, F., Horcajada, P., & Parak, W. J. (2024). Visualization of the High Surface-to-Volume Ratio of Nanomaterials and Its Consequences. *Journal of Chemical Education*, *101*(8), 3146–3155. https://doi.org/10.1021/acs.jchemed.4c00089

Prasetya, A. D., Rifai, M., & Miyamoto, H. (2020). X-ray diffraction (XRD) profile analysis of pure ECAP-annealing Nickel samples. *Journal of Physics: Conference Series*, *1436*(1), 012113. https://iopscience.iop.org/article/10.1088/1742-6596/1436/1/012113/meta

Rai, N., & Kanagaraj, S. (2022). Enhanced Antioxidant Ability of PEG-Coated $Ce_{0.5}Zr_{0.5}O_2$-Based Nanofluids for Scavenging Hydroxyl Radicals. *ACS Omega*, *7*(26), 22363–22376. https://doi.org/10.1021/acsomega.2c01266

Robkhob, P., Ghosh, S., Bellare, J., Jamdade, D., Tang, I.-M., & Thongmee, S. (2020). Effect of silver doping on antidiabetic and antioxidant potential of ZnO nanorods. *Journal of Trace Elements in Medicine and Biology*, *58*, 126448.

Rubab, M., Chelliah, R., & Oh, D.-H. (2022). Screening for Antioxidant Activity: Diphenylpicrylhydrazine (DPPH) Assay. In D. Dharumadurai (Ed.), *Methods in Actinobacteriology* (pp. 453–454). Springer US. https://doi.org/10.1007/978-1-0716-1728-1_61

Sabur, Md. A., & Gafur, Md. A. (2024). Crystallographic, Morphological, Magnetic, and Thermal Characterization of Superparamagnetic

Magnetite Nanoparticles (Fe_3O_4) Synthesized by Chemical Coprecipitation Method and Calcined at 250°C for 4 hr. *Journal of Nanomaterials*, *2024*(1), 9577778. https://doi.org/10.1155/2024/9577778

Saeed, M., Usman, M., & Haq, A. ul. (2018). Catalytic degradation of organic dyes in aqueous medium. *IntechOpen: London, UK*, *13*, 197.

Samrot, A. V., & Noel Richard Prakash, L. X. (2023). Nanoparticles induced oxidative damage in reproductive system and role of antioxidants on the induced toxicity. *Life*, *13*(3), 767.

Sanchez-Lievanos, K. R., Sun, T., Gendrich, E. A., & Knowles, K. E. (2024). Surface Adsorption and Photoinduced Degradation: A Study of Spinel Ferrite Nanomaterials for Removal of a Model Organic Pollutant from Water. *Chemistry of Materials*, *36*(9), 3981–3998. https://doi.org/10.1021/acs.chemmater.3c01986

Sangsuriyonk, K., Paradee, N., Rotjanasuworapong, K., & Sirivat, A. (2022). Synthesis and characterization of $Co_xFe_{1-x}Fe_2O_4$ nanoparticles by anionic, cationic, and non-ionic surfactant templates via co-precipitation. *Scientific Reports*, *12*(1), 4611. https://doi.org/10.1038/s41598-022-08709-9

Shah, H., Dehghani, F., Ramezan, M., Gannaban, R. B., Haque, Z. F., Rahimi, F., Abbasi, S., & Shin, A. C. (2023). Revisiting the role of vitamins and minerals in Alzheimer's disease. *Antioxidants*, *12*(2), 415.

Shenoy, R. U. K., Rama, A., Govindan, I., & Naha, A. (2022). The purview of doped nanoparticles: Insights into their biomedical applications. *OpenNano*, *8*, 100070.

Siddeeg, A., AlKehayez, N. M., Abu-Hiamed, H. A., Al-Sanea, E. A., & AL-Farga, A. M. (2021). Mode of action and determination of antioxidant activity in the dietary sources: An overview. *Saudi Journal of Biological Sciences*, *28*(3), 1633–1644. https://doi.org/10.1016/j.sjbs.2020.11.064

Singha, L. R., & Singh, R. K. L. (2020). Effect of Dopant Concentration on Structural Properties of Chemical Bath Deposited Mn-Doped PbS Nanocrystalline Thin Films. *Chalcogenide Letts*, *17*(7), 375–384.

Škrovánková, S., Mišurcová, L., & Machů, L. (2012). Antioxidant activity and protecting health effects of common medicinal plants. *Advances in Food and Nutrition Research*, *67*, 75–139.

Sohail, M., Khaliq, F., Mahmood, T., Ayub, K., Tabassum, S., & Gilani, M. A. (2021). Influence of bi-alkali metals doping over $Al_{12}N_{12}$ nanocage on stability and optoelectronic properties: A DFT investigation. *Radiation Physics and Chemistry*, *184*, 109457.

Sohel Rana, M., Azbar Rayhan, N. M., Hossain Emon, M. S., Tanvir Islam, M., Rathry, K., Mahadi Hasan, M., Mansur, M. M. I., Chakrabarty Srijon, B., Shohidul Islam, M., Ray, A., Abdur Rakib, M., Islam, A., Kudrat-E-Zahan, M., Faruk Hossen, M., & Ali Asraf, M. (2024). Antioxidant activity of Schiff base ligands using the DPPH scavenging assay: An updated review. *RSC Advances*, *14*(45), 33094–33123. https://doi.org/10.1039/D4RA04375H

Speight, J. G. (2018). *Reaction Mechanisms in Environmental Engineering: Analysis and Prediction*. Butterworth-Heinemann.

Sundram, S., Baskar, S., & Subramanian, A. (2022). Green synthesized nickel doped cobalt ferrite nanoparticles exhibit antibacterial activity and induce reactive oxygen species mediated apoptosis in MCF-7 breast cancer cells through inhibition of PI3K/Akt/mTOR pathway. *Environmental Toxicology*, *37*(12), 2877–2888. https://doi.org/10.1002/tox.23644

Tabassum, N., Anjum, R., Haque, P., Sahadat Hossain, M., Bin Mobarak, M., Saiful Quddus, M., Chowdhury, F., Rahman, L., Islam, D., Ahmed, S., & Mahmud, M. (2024). Ag–Co ferrite-based magnetic polymeric composite film: A breakthrough in cationic dye remediation for sustainable environment. *RSC Advances*, *14*(49), 36557–36575. https://doi.org/10.1039/D4RA06315E

Tahir, K., Nazir, S., Li, B., Khan, A. U., Khan, Z. U. H., Gong, P. Y., Khan, S. U., & Ahmad, A. (2015). Nerium oleander leaves extract mediated synthesis of gold nanoparticles and its antioxidant activity. *Materials Letters*, *156*, 198–201.

Tahir, W., Zeeshan, T., Waseem, S., Ali, M. D., Kayani, Z., Aftab, Z.-H., Mehtab, S. M. T., & Ezzine, S. (2023). Impact of silver substitution on the structural, magnetic, optical, and antibacterial properties of cobalt ferrite. *Scientific Reports*, *13*(1), 15730.

Thakur, P., Gahlawat, N., Punia, P., Kharbanda, S., Ravelo, B., & Thakur, A. (2022). Cobalt Nanoferrites: A Review on Synthesis, Characterization, and Applications. *Journal of Superconductivity and Novel Magnetism*, *35*(10), 2639–2669. https://doi.org/10.1007/s10948-022-06334-1

Ullah, N., Qureshi, M. T., Toufiq, A. M., Ullah, F., Al Elaimi, M., Hameed, R. S. A., Khan, A., & Ragab, H. M. E. (2021). Effect of cobalt doping on the structural, optical and antibacterial properties of α-MnO_2 nanorods. *Applied Physics A*, *127*(10), 779. https://doi.org/10.1007/s00339-021-04926-7

Valgimigli, L., & Pratt, D. A. (2015). Maximizing the Reactivity of Phenolic and Aminic Radical-Trapping Antioxidants: Just Add Nitrogen! *Accounts of Chemical Research*, *48*(4), 966–975. https://doi.org/10.1021/acs.accounts.5b00035

Vasiljevic, Z. Z., Dojcinovic, M. P., Vujancevic, J. D., Jankovic-Castvan, I., Ognjanovic, M., Tadic, N. B., Stojadinovic, S., Brankovic, G. O., & Nikolic, M. V. (2020). Photocatalytic degradation of methylene blue under natural sunlight using iron titanate nanoparticles prepared by a modified sol–gel method. *Royal Society Open Science*, *7*(9), 200708. https://doi.org/10.1098/rsos.200708

Velayutham, L., Parvathiraja, C., Anitha, D. C., Mahalakshmi, K., Jenila, M., Alasmary, F. A., Almalki, A. S., Iqbal, A., & Lai, W.-C. (2022). Photocatalytic and antibacterial activity of CoFe2O4 nanoparticles from Hibiscus rosa-sinensis plant extract. *Nanomaterials*, *12*(20), 3668.

Vinosha, P. A., Mely, L. A., Mary, G. I. N., Mahalakshmi, K., & Das, S. J. (2017). Study on cobalt ferrite nanoparticles synthesized by co-precipitation technique for photo-fenton application. *Mechanics, Materials Science & Engineering Journal*, *9*(1). https://hal.science/hal-01498330/

Xiao, X., Wang, J., Zhu, H., Liu, L., Liu, Z., & Tu, J. (2022). Effects of Nb concentration on Nb-doped anatase TiO_2: DFT + U calculations. *Physica Scripta*, *97*(5), 055819.

Zhao, Y., Zhang, X., Liu, W., Li, M., Chen, Y., Yang, Y., & Yang, S. (2024). Simple synthesis, characterization and mechanism of Fe/Zr bimetallic-organic framework for Cr (VI) removal from wastewater. *Journal of Environmental Chemical Engineering*, *12*(2), 112040. https://doi.org/10.1016/j.jece.2024.112040

Zhu, D., Bungart, B. L., Yang, X., Zhumadilov, Z., Lee, J. C.-M., & Askarova, S. (2015). Role of Membrane Biophysics in Alzheimer's—Related cell pathways. *Frontiers in Neuroscience*, *9*. https://doi.org/10.3389/fnins.2015.00186